J Stat Phys (2011) 145:313–334
DOI 10.1007/s10955-011-0299-3

Deconstructing Classical Water Models at Interfaces and in Bulk

Richard C. Remsing · Jocelyn M. Rodgers · John D. Weeks

Received: 12 May 2011 / Accepted: 30 July 2011 / Published online: 27 August 2011

Abstract Using concepts from perturbation and local molecular field theories of liquids we divide the potential of the SPC/E water model into short and long ranged parts. The short ranged parts define a minimal reference network model that captures very well the structure of the local hydrogen bond network in bulk water while ignoring effects of the remaining long ranged interactions. This deconstruction can provide insight into the different roles that the local hydrogen bond network, dispersion forces, and long ranged dipolar interactions play in determining a variety of properties of SPC/E and related classical models of water. Here we focus on the anomalous behavior of the internal pressure and the temperature dependence of the density of bulk water. We further utilize these short ranged models along with local molecular field theory to quantify the influence of these interactions on the structure of hydrophobic interfaces and the crossover from small to large scale hydration behavior. The implications of our findings for theories of hydrophobicity and possible refinements of classical water models are also discussed.

Keywords Perturbation theory · Hydrophobic interactions

1 Introduction

Classical empirical water potentials involving fixed point charges and Lennard-Jones (LJ) interactions were introduced in the first computer simulations of water forty years ago and

R.C. Remsing
Institute for Physical Science and Technology, Chemical Physics Program, University of Maryland, College Park, MD 20742, USA

J.M. Rodgers
Physical Biosciences Division, Lawrence Berkeley National Laboratory, Berkeley, CA 94720, USA

J.D. Weeks (✉)
Institute for Physical Science and Technology, Department of Chemistry and Biochemistry, Chemical Physics Program, University of Maryland, College Park, MD 20742, USA
e-mail: jdw@umd.edu

modern versions are widely used even today in many biomolecular and materials-based simulations. Two recent reviews [14, 37] have focused on this wide class of model potentials and assessed their performance for a broad range of different structural and thermodynamic properties, some of which were used as targets in the initial parameterization of the models. Despite known limitations associated with the lack of molecular flexibility and polarizability, they qualitatively and often quantitatively capture a large number of properties of water and often represent a useful compromise between physical realism and computational tractability.

Given the simple functional forms of the intermolecular potentials it may seem surprising that such good agreement is possible. But recent work has shown that even simpler models where particles interact via isotropic repulsive potentials with two distinct length scales are able to qualitatively reproduce certain characteristic dynamic and thermodynamic anomalies of bulk water [8, 42, 43]. Similarly in dense uniform simple liquids a hard-sphere-like repulsive force reference system can give a good description of the liquid structure, and this in turn permits thermodynamic properties to be determined by a simple perturbation theory [15, 40].

This suggests it should be useful to analyze the construction and predictions of empirical water potentials from the perspective of perturbation theory of uniform fluids and the related Local Molecular Field (LMF) theory [10, 11, 28, 29, 39, 40]. LMF theory provides a more general approach applicable to both uniform and nonuniform fluids and gives strong support to the basic idea of perturbation theory that in a uniform fluid slowly varying long ranged parts of the intermolecular interactions have little effect on the local liquid structure.

To apply these ideas to water we divide the intermolecular interactions in a given water model into appropriately chosen short and long ranged parts. In this context, it is conceptually useful to consider separately the slowly varying long ranged parts of both the LJ interactions and the Coulomb interactions. This deconstruction of the water potential via LMF theory provides a hierarchical framework for assessing separately the contributions of (i) strong short ranged interactions leading to the local hydrogen bonding network, (ii) dispersive attractions between water molecules, and (iii) long ranged dipolar interactions between molecules. Disentangling these contributions without the insight of LMF theory is very difficult due to the *multiple* contributions of the point charges and the LJ interactions in standard molecular water models.

In uniform systems, the long ranged forces on a given water molecule from more distant neighbors tend to cancel [40, 41]. The remaining strong short ranged forces between nearest neighbors arise from the interplay between the repulsive LJ core forces and the short ranged attractive Coulomb forces between donor and acceptor charges. These forces determine a minimal reference model that can accurately describe the local liquid structure—the hydrogen-bond network for bulk water. The slowly varying parts of the intermolecular interactions are not important for this local structure and could be varied essentially independently to help in the determination of other properties as is implicitly done in the full model. Based on previous work with LMF theory [28, 30, 31], we examine two basic areas where we expect the different contributions to play varying but important roles—bulk thermodynamics and nonuniform structure. The short ranged interactions responsible for the hydrogen-bonding network are clearly necessary in all cases. LMF theory allows us to determine the relative importance of dispersive attractions and long-ranged dipolar attractions in these applications using simple analytical corrections for thermodynamics and an effective external field for nonuniform structure.

In the next section we discuss the separation of the water potential into short and long ranged parts and show that a minimal short ranged reference model can very accurately describe atom-atom correlation functions and other properties of the hydrogen bond network

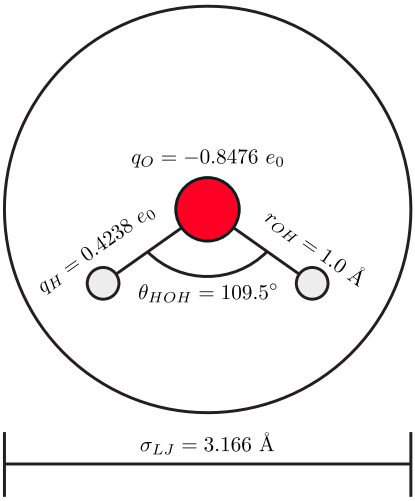

Fig. 1 (Color online) Schematic diagram of the SPC/E water model listing its various geometric parameters and interaction parameters. The O–H bond length and H–O–H angle are fixed, such that the molecule is rigid. The LJ well depth is $\epsilon_{\mathrm{LJ}} = 0.65$ kJ/mol. The oxygen site is depicted as a large *red circle*, while the hydrogen atoms are shown as smaller, *gray circles*

in bulk water. In Sect. 3 we examine the thermodynamic implications of this picture, focusing on two anomalous properties of bulk water qualitatively well described by the full water model, the density maximum at one atmosphere pressure and the behavior of the "internal pressure" $(\partial E/\partial V)_T$, which has a temperature and density dependence opposite to that of most organic solvents. Then in Sect. 4 we look at the effects of the unbalanced long-ranged electrostatic and dispersion forces at aqueous interfaces. LMF theory reveals strong similarities between the behavior of water at the liquid-vapor interface and a planar hydrophobic wall, consistent with previous work, and provides new insight into the relative importance of electrostatic and dispersion forces and the transition from small to large scale hydrophobicity as the radius of a nonpolar solute is increased.

2 Local Hydrogen Bonds in Full and Truncated Water Potentials

In this paper we consider one of the simplest and most widely used water models, the extended simple point charge (SPC/E) model [6], but similar ideas and conclusions apply immediately to most other members of this class. As shown in Fig. 1, SPC/E water consists of a LJ potential as well as a negative point charge centered at the oxygen site. Positive point charges are fixed at hydrogen sites displaced from the center at a distance of 1 Å with a tetrahedral HOH bond angle. It is a remarkable fact that this simple model can reproduce many structural, thermodynamic, and dielectric properties of bulk water as well as those of water in nonuniform environments around a variety of solutes and at the liquid-vapor interface.

In the following we use the perspective of perturbation and LMF theory to help us see how this comes about. We use these ideas here not to suggest more efficient simulations using short ranged model potentials but rather as a method of analysis that provides physical insight into features of the full model as well. Since a detailed description and justification of LMF theory is given elsewhere [29], we will focus on qualitative arguments and just quote specific results when needed.

Figure 2 gives some insight into why a perturbation picture based on the dominance of strong short ranged forces in uniform environments could be especially accurate for bulk SPC/E and related water models. This shows two adjacent water molecules with a separation

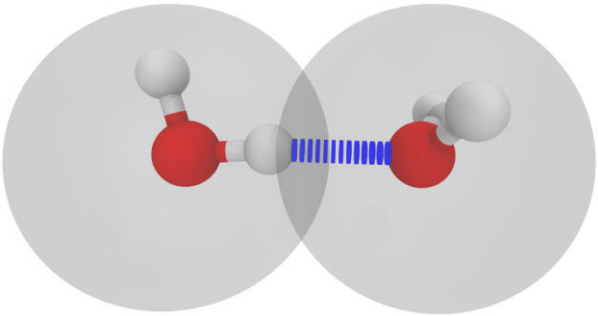

Fig. 2 (Color online) Optimal hydrogen bonding configuration of water taken from two molecules in ice Ih. LJ cores are depicted as gray transparent spheres with a diameter $\sigma_{LJ} = 3.16$ Å, while the hydrogen bond between waters with oxygens separated by 2.75 Å is illustrated by a *dashed, blue cylinder*. Oxygen and hydrogen atoms are colored *red* and *white*, respectively

of 2.75 Å that form an optimal hydrogen bond as seen in the structure of ice Ih. Hydrogen bonding in this model is driven by the very strong attractive force between opposite charges on the hydrogen and oxygen sites of adjacent properly oriented molecules. Proper orientation permits similar strong bonds to form with other molecules, leading to a tetrahedral network in bulk water. The gray circles drawn to scale depict the repulsive LJ core size as described by the usual parameter $\sigma_{LJ} = 3.16$ Å. The substantial overlap indicates a large repulsive core force opposing the strong electrostatic attraction, finally resulting in a nearest neighbor maximum in the equilibrium oxygen-oxygen correlation function of 2.75 Å.

It is interesting to note that the first BNS water model introduced in 1970 used a smaller core size $\sigma_{LJ} = 2.82$ Å [4]. However a much larger LJ core with strong core overlap at typical hydrogen-bond distances is a common property of almost every water model introduced since then and seems to be a key feature needed to get generally accurate results from simple classical point charge models. Evidentially the highly fluctuating local hydrogen-bond network in these models arises from geometrically-frustrated "charge pairing", where the strong LJ core repulsions and the presence of other charges on the acceptor water molecule oppose the close approach of the strongly-coupled donor and acceptor charges.

We can test the accuracy of this picture by considering various truncated or "short" water models where slowly varying long ranged parts of the Coulomb and LJ interactions in SPC/E water are completely neglected. We first consider a Gaussian-truncated (GT) water model, already studied by LMF theory [28, 30, 31]. Here the Coulomb potential is separated into short and long ranged parts as

$$v(r) = \frac{1}{r} = \frac{\mathrm{erfc}(r/\sigma)}{r} + \frac{\mathrm{erf}(r/\sigma)}{r} = v_0(r) + v_1(r), \tag{1}$$

where erf and erfc are the error function and complementary error function, respectively. The short-ranged $v_0(r)$ is the screened electrostatic potential resulting from a point charge surrounded by a neutralizing Gaussian charge distribution of width σ. Hence $v_0(r)$ vanishes rapidly at distances r much greater than σ while at distances less than σ the force from $v_0(r)$ approaches that of the full $1/r$ potential.

In GT water, depicted in Fig. 3a, the Coulomb potential associated with each charged site in SPC/E water is replaced by the short-ranged v_0 with no change in the LJ interaction. As suggested by Fig. 2, important features of the local hydrogen-bond network should be well captured by such a truncated model if the cutoff distance controlled by the length parameter σ in (1) is chosen larger than the hydrogen bond distance. Following Refs. [31] and [30], here we make a relatively conservative choice of $\sigma = 4.5$ Å, but values as small as 3 Å give essentially the same results. The circles are drawn to scale with diameters σ and σ_{LJ}.

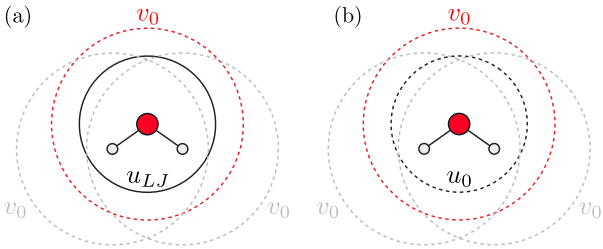

Fig. 3 (Color online) Schematic diagrams of (**a**) GT and (**b**) GTRC water models. Truncated interactions are indicated by *dashed lines*, while full interaction potentials are indicated by *solid lines*. LJ interactions are represented by *black lines*, while oxygen and hydrogen electrostatic interaction potentials are shown as *red* and *gray lines*, respectively

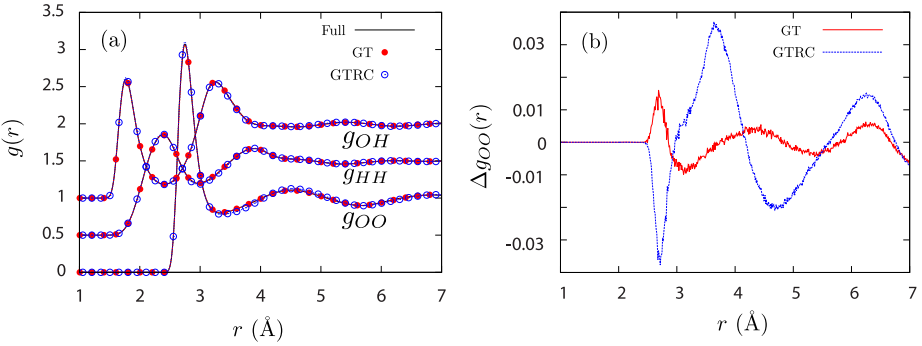

Fig. 4 (Color online) (**a**) Oxygen-oxygen, oxygen-hydrogen, and hydrogen-hydrogen site-site pair distribution functions, $g_{\mathrm{OO}}(r)$, $g_{\mathrm{OH}}(r)$, and $g_{\mathrm{HH}}(r)$, respectively, for the three water models under study at $T = 300$ K and $v = 30.148$ Å^3. g_{HH} and g_{OH} have been shifted by 0.5 and 1 units, respectively, for clarity. (**b**) Differences between $g_{\mathrm{OO}}(r)$ of the full model and that of the designated reference systems, $\Delta g_{\mathrm{OO}}(r)$

The basic competition between very strong short ranged repulsive and attractive forces in the hydrogen bond depicted in Fig. 2 should be captured nearly as well by an even simpler reference model where the LJ potential is truncated as well, and replaced by the repulsive force reference potential $u_0(r)$ used in the WCA perturbation theory for the LJ fluid [40]. The resulting Gaussian truncated repulsive core (GTRC) model is schematically shown in Fig. 3b.

As discussed in perturbation theories of simple liquids [15, 40], a well-chosen reference system should accurately reproduce bulk structure present in the full system at the same fixed density and temperature. As illustrated by the pair distribution functions in Fig. 4, bulk GT and GTRC water models have a liquid state structure virtually identical to that in the full SPC/E model. This very good agreement is also reflected in other properties of the hydrogen-bond network. We directly examined the hydrogen bonding capabilities of GT and GTRC water models through the calculation of the average number of hydrogen bonds per water molecule, $\langle n_{\mathrm{HB}} \rangle$, as well as the probability distribution of a water molecule taking part in n_{HB} hydrogen bonds, $P(n_{\mathrm{HB}})$, using a standard distance criterion of hydrogen bonds, $R_{\mathrm{OO}} < 3.5$ Å and $\theta_{\mathrm{HOO'}} < 30°$, where R_{OO} is the oxygen-oxygen distance and $\theta_{\mathrm{HOO'}}$ is the angle formed by the H–O bond vector on the hydrogen bond *donating* water molecule and the O–O′ vector between the oxygen on the donor water (O) and the acceptor oxygen (O′) [25]. For both GT and GTRC water models, $\langle n_{\mathrm{HB}} \rangle$ and $P(n_{\mathrm{HB}})$ were calculated at temperatures

ranging from 220–300 K, and were found to be nearly identical to the analogous quantities in the full SPC/E model (data not shown). These findings give credence to the idea that these two truncated models reproduce the hydrogen-bond network of the full model to a high degree of accuracy.

These truncated models offer a minimal structural representation of bulk water as a fluctuating network of short ranged bonds determined mainly by the balance between the very strong electrostatic attraction between donor and acceptor charges and the very strong repulsion of the overlapping LJ cores. We can view them as primitive water models in their own right, analogous to other simplified models recently proposed, which capture very well arguably the most important structural feature of bulk water, the hydrogen bond network, and it is instructive to see what other properties of water such minimal network models can describe. But corrections from neglected parts of the intermolecular interactions are certainly needed for bulk thermodynamic and dielectric properties and for both structure and thermodynamics of water in nonuniform environments. LMF theory provides a more general framework where the truncated models are viewed as useful reference systems that can be systematically corrected to achieve good agreement with full water models. We will use both viewpoints in the next section.

3 Thermodynamic Anomalies of Bulk Water Using Full and Truncated Water Potentials

3.1 Density Maximum

Now we turn our attention to the thermodynamics of bulk water. For a fixed volume V, temperature T, and number of molecules N, the pressure and other thermodynamic properties of the GT and GTRC systems will not generally equal those of the full system. However, because of the accurate reference structure, we can correct the thermodynamics using simple mean-field (MF) arguments. Thus we can define the pressure in the full system to be the sum of the short-ranged reference pressure and a long-ranged correction, $P = P_0 + P_1$.

Simple corrections to the energy and pressure of the GT model from this perspective were recently derived [30]. With $\sigma = 4.5$ Å, these corrections are relatively small and were ignored in most earlier work using truncated water models but they are conceptually important in revealing the connections between truncated models and perturbation theory and are required for quantitative agreement. The pressure correction $P_1 = P_1^q$ for the GT model arises only from long-ranged Coulomb interactions and is given as

$$P_1^q = -\frac{k_B T}{2\pi^{3/2}\sigma^3}\frac{\epsilon - 1}{\epsilon}, \tag{2}$$

where ϵ is the dielectric constant.

In the case of the GTRC model, the need for a thermodynamic correction is much more obvious since we have to correct for the absence of LJ attractions as well. Here we adopt the simple analytic correction used in the van der Waals (vdW) equation derived from WCA theory for the LJ fluid, as discussed in Ref. [39]. Thus $P_1 = P_1^q - a\rho^2$ for the GTRC potential, where

$$a \equiv -\frac{1}{2}\int d\mathbf{r}_2\, u_1(r_{12}) \tag{3}$$

and u_1 is attractive part of the LJ potential. This simple approximation does not give quantitative results but does capture the main qualitative features and we use it here to emphasize

the point that both the long ranged Coulomb and dispersion force corrections to bulk GTRC water can be treated by simple perturbation methods.

We can test the accuracy of these corrections by using them to help determine the temperature T_{MD} at which the density maximum of the full SPC/E water model at a constant pressure of 1 atm should occur. This can alternatively be defined as the temperature at which the thermal expansion coefficient, α_P, is zero. Accordingly, we seek to evaluate α_P using the relation

$$\alpha_P \equiv \frac{1}{v}\left(\frac{\partial v}{\partial T}\right)_P = -\frac{1}{v}\left(\frac{\partial P}{\partial T}\right)_v \left(\frac{\partial v}{\partial P}\right)_T, \tag{4}$$

where $v = V/N$ is the volume per particle. Using the last expression we can determine where the quantity $(\partial P/\partial T)_v = 0$ by monitoring the corrected pressure of the reference systems while changing the temperature at a fixed density. This can be done by simulation in the canonical ensemble. The fixed density ensures that the structure of the reference and full systems are very similar, as assumed in the derivation of the corrections in (2) and (3). We can also determine T_{MD} through the first equality in (4) by finding where $(\partial v/\partial T)_P = 0$. Thus we simulate GT and GTRC water at constant pressures of $P_0 = P - P_1$, where $P =$ 1.0 atm is the pressure in the full system. Note that the correction $P_1^q \equiv P_1^q(T; \epsilon(T))$ is temperature-dependent, as is the dielectric constant ϵ, so that we are not moving along an isobar in P_0, but an isobar in P. The temperature-dependent values of ϵ were taken to be the experimental values [16].

Figures 5a and 5b give the density and pressure of full SPC/E water and the corrected reference models as a function of temperature. As expected, the inclusion of P_1^q in the pressure of GT water quantitatively corrects the density and pressure of this system. However, the MF correction applied to GTRC water, $P_0 = P - P_1^q + a\rho^2$, is not as accurate, although the dependence of ρ on T is qualitatively well captured. These remaining errors arise from our use of the simple van der Waals $a\rho^2$ correction for the long ranged part of the LJ potential. This level of agreement is typical when this correction is used in pure LJ fluids [39] and a full WCA perturbative treatment of the attractive portion of the LJ potential in GTRC water would likely lead to quantitatively accurate results [40].

We now turn to the alternate and less accurate interpretation of the GT and GTRC models as primitive water models in their own right. Do these models at an uncorrected pressure of 1 atm have a density maximum and how well does it compare to that of the full model? To that end, we find where $(\partial v/\partial T)_P = 0$ in each model by varying the temperature along an isobar using MD simulations in the isothermal-isobaric ensemble at a constant pressure of 1 atm. By requiring the same pressure in the full and reference models, we probe structurally different state points in general and there is no guarantee that the density and temperature of the reference systems at a density maxima (if present) will be similar to that in the full system. Nevertheless Fig. 5c shows that the GT model does have a density maximum very similar to that of the full model. This is because the pressure correction to the density from the long-ranged Coulomb interactions in (2) is very small on the scale of the graph. In contrast, the uncorrected GTRC model does not exhibit a density maximum at $P = 1.0$ atm, even upon cooling to 50 K (data not shown).

These results should be compared to earlier work where the TIP4P water potential was approximated by a simpler "primitive model" [20]. In that work, the repulsive LJ core was mapped onto a hard-sphere potential, hydrogen bonding was captured by a square-well potential, and long-ranged dipole-dipole interactions were represented with a dipolar potential. The equation of state was found using a perturbative approach, and thermodynamic quantities were analyzed. The authors of Ref. [20] found that the inclusion of dispersion forces

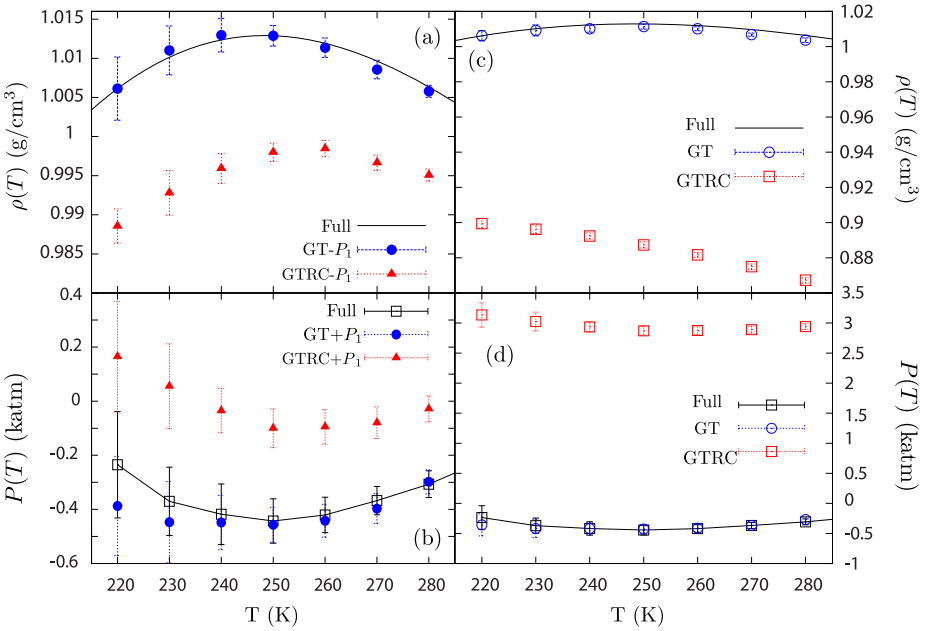

Fig. 5 (Color online) The dependence of (**a**) density and (**b**) pressure for the corrected reference models as a function of temperature. The analogous quantities for the models without MF corrections are shown in (**c**) and (**d**), respectively. $\rho(T)$ is calculated at a constant pressure of 1.0 atm and $P(T)$ is calculated at a fixed volume of $v = 30.148$ Å^3. Full SPC/E data for $\rho(T)$ at constant P was taken from the work of Ashbaugh et al. [3]

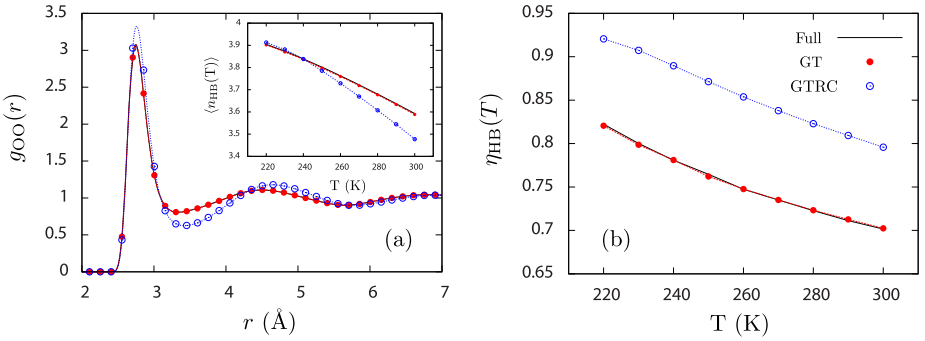

Fig. 6 (Color online) (**a**) The oxygen-oxygen pair distribution function, $g_{OO}(r)$, for the three water models at $T = 300$ K. *Inset*: The average number of hydrogen bonds per water molecule as a function of temperature, $\langle n_{HB}(T)\rangle$, for full and truncated water models. (**b**) Hydrogen bonding efficiency η_{HB} as a function of temperature. All results were obtained at a constant uncorrected pressure of 1 atm

does not lead to a density maximum, and only when both dispersive interactions and long-ranged dipole-dipole interactions were taken into account did a density maximum appear.

To provide some understanding of these differing results, we analyze the structure of the uncorrected GT and GTRC reference models in comparison to the full model at the common pressure of one atmosphere. The oxygen-oxygen radial distribution functions, $g_{OO}(r)$, for each of the three water models at $T = 300$ K are depicted in Fig. 6a. The GT model is in

good agreement with the full model, consistent with its accurate description of the bulk water density and the density maximum. In contrast, as shown later in Fig. 9, the coexisting liquid density of GTRC water is about 15% lower than that of the full water model. Nevertheless the first peak of $g_{OO}(r)$ in GTRC water is *higher* than that of the full water model due to better formation of local hydrogen bonds. As shown in the inset, a molecule of GTRC water has slightly fewer hydrogen bonds on average than full and GT water models for temperatures higher than 240 K. However the hydrogen bond efficiency shown in Fig. 6b,

$$\eta_{HB} = \frac{\langle n_{HB} \rangle}{\langle n_{NN} \rangle}, \tag{5}$$

where $\langle n_{NN} \rangle$ is the average number of nearest-neighbors satisfying $R_{OO} < 3.5$ Å, indicates that GTRC water is about 10 percent more efficiently hydrogen bonded to its available neighbors at all temperatures. In this sense the low density GTRC water at $P = 1.0$ atm is structurally more ice-like than the full water model.

These results provide some insight into earlier first principles simulations of liquid water using density functional theory [21, 32, 38]. The standard exchange-correlation functionals used there can give a good description of local hydrogen bonding, but do not include effects of van der Waals interactions. These simulations produced a decrease in the bulk density of water accompanied by increased local structural order very similar to that seen here for GTRC water. Moreover, when dispersive interactions were crudely accounted for, they observed much better agreement with experiment, in complete agreement with our findings for perturbation-corrected GTRC water.

Our results indicate that van der Waals attractions play the role of a cohesive energy needed to achieve the high density present in SPC/E water at low pressure, as demonstrated by the qualitative accuracy of (3) and the good agreement of the GT model. Evidentially a density maximum can arise only when additional somewhat less favorably bonded molecules are incorporated into the GTRC network to produce the full water density. If the local hydrogen bond network of water at the correct bulk density is properly described, long ranged dipolar forces are not needed to obtain the correct behavior of $\rho(T)$. Indeed, LJ attractions are not needed either provided that the proper bulk density is prescribed by some other means. Thus we found that if GTRC water is kept at a high constant pressure of 3 katm, where its bulk density is close to that of the full water model at ambient conditions, a density maximum is also observed (data not shown).

3.2 Internal Pressure

We further employ the reference water models to explain the anomalous "internal pressure" of water [33]. For a typical van der Waals liquid, the internal pressure is given by $P_i = (\partial\varepsilon/\partial v)_T \approx a\rho^2$ for low to moderate densities, where $\varepsilon = E/N$ is the energy per molecule. In fact, it was recently shown by computer simulation that the portion of the internal pressure due to the attractions in a LJ fluid displays this $a\rho^2$ dependence even at high densities [13]. Water, on the other hand, displays a negative dependence of P_i on density. It is this anomalous behavior that we seek to explain.

We begin by partitioning the internal energy of the system as

$$\varepsilon = \varepsilon^{LJ} + \varepsilon^{q}, \tag{6}$$

where ε^{LJ} is the Lennard-Jones contribution to the energy and ε^{q} is the energy due to charge-charge interactions (note that the change in kinetic energy when perturbing the volume at

constant T is zero, so we only consider the potential energy). We can then write the internal pressure as

$$P_i = \left(\frac{\partial \varepsilon}{\partial v}\right)_T = P_i^{\mathrm{LJ}} + P_i^q. \tag{7}$$

This decomposition of P_i will allow us to determine which molecular interactions are responsible for the strange dependence of this quantity on ρ.

Figure 2 suggests the following qualitative picture. At a given temperature and density the dominant hydrogen bond contribution to the energy ε is determined from the balance between strong repulsive forces from the LJ cores and strong attractions from the more slowly varying Coulomb interactions between donor and acceptor charges. The Coulomb contribution P_i^q to the internal pressure $P_i(T, \rho)$ is positive since a small positive change in volume reduces the negative Coulomb energy and similarly the LJ core contribution to P_i^{LJ} is negative. If the density is now varied at constant temperature we would expect the changes in $P_i(T, \rho)$ to be dominated by the rapidly varying LJ core forces.

Conversely, to the extent that the repulsive LJ cores are like hard spheres, they would contribute no temperature dependence to the internal pressure at fixed density. Thus we expect the more slowly varying Coulomb forces to largely determine how the internal pressure varies with temperature at fixed density. The results given below are in complete agreement with these expectations.

We evaluated (7) by performing MD simulations of water in the canonical ensemble for various volumes at $T = 300$ K. The dependence of the internal pressure on density at $T = 300$ K is shown in Fig. 7. Note that the total internal pressure, P_i, becomes increasingly negative as ρ is increased, in direct opposition to the $a\rho^2$ dependence given by the vdW equation of state. However, it is known that as the density of a LJ fluid is increased to high values so that neighboring repulsive cores begin to overlap, the total P_i exhibits a maximum, after which the internal pressure becomes increasingly negative from the dominant contribution of the repulsive interactions [13].

As shown in Fig. 2 there is substantial overlap of the repulsive LJ cores between nearest neighbors in SPC/E water. The repulsive interactions from these LJ cores dominate the density dependence of both ε and P_i for SPC/E and related water models, as evidenced by the similarity of the internal pressures of both the full and GTRC water models in Fig. 7. Although $\varepsilon^q > \varepsilon^{\mathrm{LJ}}$ for all density, ε^q does not exhibit very large changes upon increasing density, a direct consequence of the ability of water to maintain its hydrogen bond network under the conditions studied. Thus the density dependence of the internal pressure of SPC/E water is actually similar to that of a LJ fluid but one at a very high effective density with substantial overlap of neighboring cores.

In addition to the anomalous density dependence of P_i, the temperature dependence of the internal pressure of water has also been called an anomaly [33]. For most organic liquids (and vdW fluids), the internal pressure decreases with increasing temperature, but that of water increases when the temperature is increased, as shown in Fig. 8. Using the concepts presented above, we can rationalize this behavior in terms of molecular interactions. By decomposing P_i into its electrostatic and LJ components, we find that P_i^q dominates the temperature dependence of the internal pressure, increasing with increasing temperature, while P_i^{LJ} is dominated by repulsive interactions at all temperatures studied, as evidenced by its negative value for all T. As the temperature of the system is increased, the number of ideally tetrahedrally coordinated water molecules decreases, and the hydrogen bond network becomes increasingly "flexible". Therefore, if one increases the volume of the system at high T, water will more readily expand to fill that volume. But an increase in the

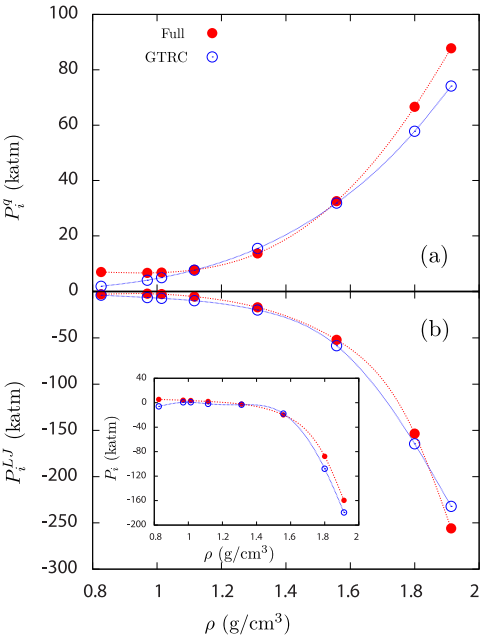

Fig. 7 (Color online) (**a**) The electrostatic contribution to the internal pressure, P_i^q, and (**b**) the analogous contribution from LJ interactions, P_i^{LJ}. The total internal pressure as a function of density is shown in the *inset*. *Lines* are guides to the eye

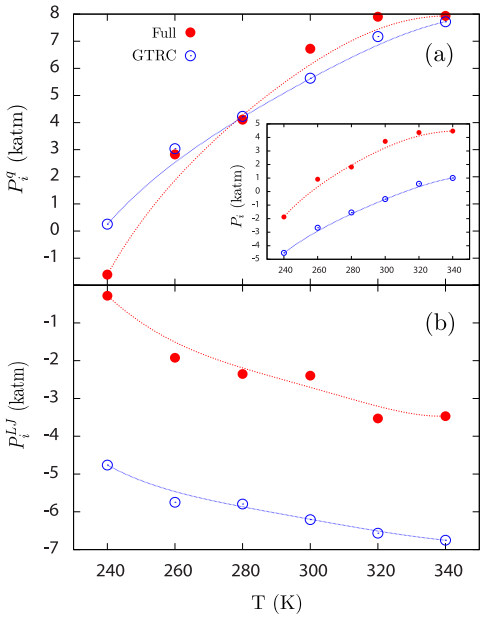

Fig. 8 (Color online) (**a**) The electrostatic contribution to the internal pressure, P_i^q, and (**b**) the analogous contribution from LJ interactions, P_i^{LJ}, both as a function of temperature at a fixed volume of $v = 29.9$ Å^3. The total internal pressure as a function of temperature is shown in the *inset*. *Lines* are guides to the eye

electrostatic energy will also occur due to a slight decrease in the number of (favorable) hydrogen bonding interactions. This will happen to a lesser extent at low temperatures, when the hydrogen bond network is more rigid and the thermal expansivity of water is lower.

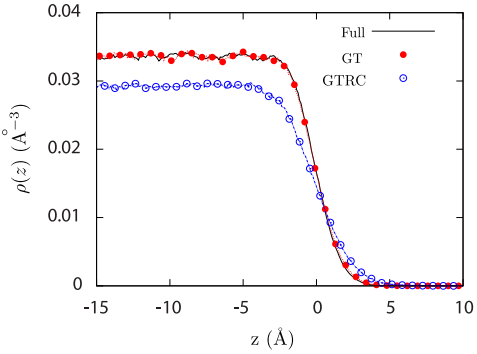

Fig. 9 (Color online) Density profiles of oxygen sites at the liquid-vapor interface of Full, GT, and GTRC water models. The Gibbs dividing surface of each interface is located at $z = 0$ Å

4 Unbalanced Forces in Nonuniform Aqueous Media from the Viewpoint of LMF Theory

In contrast to uniform systems, a net cancellation of long ranged forces does not occur in nonuniform environments, and these unbalanced forces can cause significant changes in the structure and thermodynamics of the system [28, 39]. As shown above, the bulk structure of both the GT and GTRC models are very similar to that of the full water model at a given temperature and density. But interfacial structure and coexistence thermodynamic properties of the uncorrected reference models can be very different. For example, GTRC water still has a self-maintained liquid-vapor (LV) interface at $T = 300$ K as illustrated in Fig. 9, even though the LJ attractions are ignored, because of the strong charge pairing leading to hydrogen bond formation. However its 90–10% interfacial width increases to $w \approx 4.9$ Å from the $w \approx 3.5$ Å seen in both GT water and the full water model, and the coexisting liquid density of GTRC water is about 15% lower. In contrast, the density profile of the GT model with LJ interactions fully accounted for is in very good qualitative agreement with that of the full model. This strongly suggests that if local hydrogen bonding is properly taken into account, the equilibrium structure of the LV interface of water is governed mainly by long ranged LJ attractions, with long ranged dipole-dipole interactions playing a much smaller role. It is the exact balance of these long ranged interactions we seek to examine in this section.

LMF theory provides a framework in which the averaged effects of long ranged forces are accounted for by an effective external field [29]. It has previously been used mainly as a computational tool to permit very accurate determination of properties of the full nonuniform system while using a numerical simulation of the short ranged reference system in the presence of the effective field [11, 12, 28]. But the effective or renormalized field also gives a convenient and natural measure of the importance of long ranged forces in different environments. In this section we use the renormalized external fields determined directly from simulations of interfaces in the full SPC/E water model along with simulations of truncated water models to quantitatively examine the relative influence of the local hydrogen bond network and unbalanced long-ranged Coulomb and van der Waals forces.

4.1 Water-Vapor and Water-Solid Interfaces

We first consider the LV interfaces of the SPC/E, GT, and GTRC water models shown in Fig. 9. The removal of long-ranged electrostatics in the GT model leaves the density distribution virtually unchanged, whereas removal of the LJ attractions in GTRC water has a substantial impact on $\rho(z)$. To understand this behavior, we focus our attention on the impact

of the averaged unbalanced forces from the long-ranged electrostatic and LJ interactions, as determined in LMF theory from the effective external fields $\mathcal{V}_{\mathrm{R1}}$ and $\phi_{\mathrm{R1}}^{\mathrm{LJ}}$, respectively and defined below. The unbalanced force $\mathcal{F}$ acting on an oxygen site from the LMF potentials is given by

$$\mathcal{F}_{\mathrm{O}}(\mathbf{r}) = -\nabla_{\mathbf{r}}\phi_{\mathrm{R1}}^{\mathrm{LJ}}(\mathbf{r}) - q_{\mathrm{O}}\nabla_{\mathbf{r}}\mathcal{V}_{\mathrm{R1}}(\mathbf{r}). \tag{8}$$

Here q_{O} is the partial charge on the oxygen site and $\mathcal{V}_{\mathrm{R1}}(\mathbf{r})$ is the slowly-varying part of the effective electrostatic field, given by

$$\mathcal{V}_{\mathrm{R1}}(\mathbf{r}) = \frac{1}{\epsilon}\int d\mathbf{r}'\,\rho^{q}(\mathbf{r}')v_1\big(|\mathbf{r}-\mathbf{r}'|\big), \tag{9}$$

where $\rho^{q}(\mathbf{r})$ is the total charge density of the system. The other contribution $\phi_{\mathrm{R1}}^{\mathrm{LJ}}(\mathbf{r})$ is the field arising from the unbalanced LJ attractions on the oxygen site (where the LJ core is centered), given by

$$\phi_{\mathrm{R1}}^{\mathrm{LJ}}(\mathbf{r}) = \int d\mathbf{r}'\big[\rho(\mathbf{r}') - \rho^{\mathrm{B}}\big]u_1\big(|\mathbf{r}-\mathbf{r}'|\big), \tag{10}$$

with $\rho(\mathbf{r})$ indicating the nonuniform singlet density distribution of oxygen sites and ρ^{B} defined as the bulk density of oxygen sites at the state point of interest [29, 39]. Since the hydrogen sites lack LJ interactions, the unbalanced LMF force acting on a hydrogen site is due exclusively to electrostatics,

$$\mathcal{F}_{\mathrm{H}}(\mathbf{r}) = -q_{\mathrm{H}}\nabla_{\mathbf{r}}\mathcal{V}_{\mathrm{R1}}(\mathbf{r}). \tag{11}$$

Given its importance in the density distribution of water, it may seem natural to examine the components of the LMF force on the oxygen sites, $\mathcal{F}_{\mathrm{O}}(z)$, shown in the inset of Fig. 10a. Naive examination of the relative magnitude of these force functions would lead to the conclusion that long-ranged electrostatics are the dominant unbalanced force at the LV interface. However, $\mathcal{V}_{\mathrm{R1}}$ also interacts with hydrogen sites and one should instead consider the net forces from long ranged Coulomb and LJ interaction felt by an entire water *molecule* at these interfaces.

This ensemble averaged net molecular force $\langle\mathcal{F}\rangle$ (Fig. 10b) clearly indicates that the net unbalanced force at an interface is almost entirely due to long-ranged LJ attractions from the bulk, which pull water molecules away from the interface. The long-ranged Coulomb contributions to the average force on a water molecule are essentially negligible in comparison. This is not surprising since water molecules are neutral, and it has previously been shown that the small net interfacial electrostatic force simply provides a slight torque on water molecules in this region [28]. This torque has little effect on the oxygen density distribution, as illustrated by the good agreement of the GT model density profile with that of the full water model in Fig. 9. However, it plays a key role in determining electrostatic and dielectric properties, which are strongly affected by the behavior of the total charge density, and here the uncorrected GT model gives very poor results [28, 29].

It is also instructive to compare the unbalanced long ranged forces at the LV interface to those at the liquid-solid (LS) interface between water and a model hydrophobic 9-3 LJ wall introduced by Rossky and coworkers [23], as shown in Fig. 10b. Despite the large differences in the density profiles shown in Fig. 10a, the net unbalanced forces on molecules at the LV and LS interfaces are remarkably similar for all z until molecules encounter the

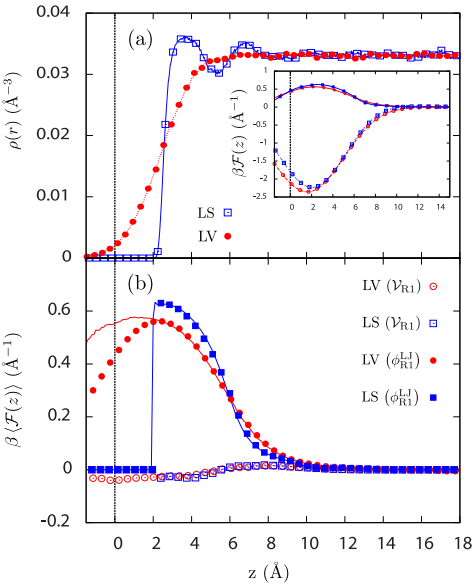

Fig. 10 (Color online) (**a**) Density distributions as a function of the z-coordinate for the hydrophobic LS interface and the LV interface of water. (**b**) Ensemble averaged net force on a water *molecule* due to $\mathcal{V}_{R1}$ (*open symbols*) and ϕ^{LJ}_{R1} (*closed symbols*) at the LV (*circles*) and LS (*squares*) interfaces and the density profiles of the two systems. *Solid lines* indicate the net force due to u_1. The *black dashed line* at $z = 0$ Å indicates the position of the hydrophobic wall. The Gibbs dividing interface of the LV system is located at $z = 2.34$ Å, in order to make comparison with the water-wall interface. *Inset*: Forces on oxygen sites only, determined by evaluating the gradient of the corresponding LMF potentials. Labeling for the *inset* is the same as that in (**b**)

harsh repulsion of the wall and an accurate sampling of $\langle\mathcal{F}(z)\rangle$ by simulation cannot be made. Water molecules can sample all regions in the liquid-vapor interface, leading to a smooth $\langle\mathcal{F}(z)\rangle$ at smaller z.

Indeed, the net molecular force due explicitly to a configurational average of the attractive $u_1(r)$ acting on molecules present at each z-position is in outstanding quantitative agreement with that arising from $\phi^{LJ}_{R1}(z)$ for all adequately sampled regions in the liquid, as illustrated by the solid lines in Fig. 10b. This serves largely as confirmation of the validity of the mean-field treatment inherent in LMF theory within the liquid slabs. Deviations between the two quantities for distances less than the Gibbs dividing surface are a reflection of the increasing effect of larger force fluctuations due to long-wavelength capillary waves not well described by mean field theory. The relative magnitudes of the components of $\langle\mathcal{F}\rangle$ for the LV and LS interfaces are strikingly similar, with the net unbalanced LJ force $\langle\mathcal{F}(z;\phi^{LJ}_{R1})\rangle$ reaching its maximum value of slightly less than $k_BT/$Å near the Gibbs dividing interface and the repulsive boundary of the wall, respectively.

The similarities of the unbalanced forces at the LV and the hydrophobic LS interfaces of water and the dominance of the LJ attractions are completely consistent with the analogies commonly drawn between these two systems [7, 9, 35] and used in the LCW theory of hydrophobicity [24, 36, 39]. A common criticism of LCW theory is its apparent neglect of the hydrogen bond network of water and the use of a van der Waals like expression for the unbalanced force at an interface. Although some features of the network are implicitly captured by using the experimental surface tension and radial distribution function of water as

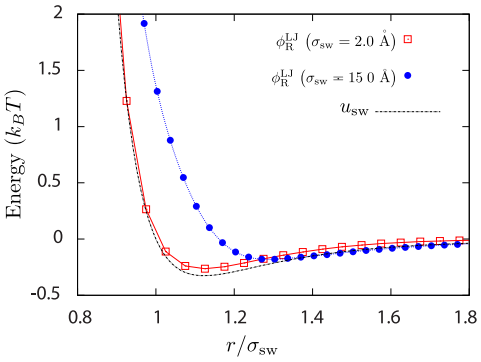

Fig. 11 (Color online) Comparison of renormalized solute-water vdW potentials for $\sigma_{sw} = 2.0$ Å (*squares*) and $\sigma_{sw} = 15.0$ Å (*circles*). The full solute-water LJ potential u_{sw} is also shown for comparison (*black dash-dot line*). Note that the x-axis is scaled by the solute-water interaction length-scale σ_{sw}

input to the theory, electrostatic effects at the interface, including dipole-dipole interactions, are ignored. However, this assumption is justified since the averaged effects of long-ranged dipole-dipole interactions, accounted for by $\mathcal{V}_{R1}$, are shown to indeed be negligible at a hydrophobic interface (Fig. 10). LCW theory correctly describes the unbalanced LJ attractions from the bulk, which dominates the behavior at both the liquid-vapor and extended hydrophobic interfaces.

4.2 Crossover from Small to Large Length Scale Hydration

LCW theory combined the idea of unbalanced forces with experimental data in water to predict a crossover in the solvation of spherical hydrophobic solutes occurring at a radius of about 1 nm [24]. While the local hydrogen bond network can be maintained around smaller solutes, some bonds must be broken on larger length scales, leading to an enthalpically dominated regime [7, 9, 35]. Here we use LMF theory and a direct analysis of the unbalanced long ranged forces to provide further physical insight into how this crossover comes about. We study the hydration of spherical hydrophobic solutes, which interact with the oxygen site of water via a solute-water LJ potential $u_{sw}(r)$ with a fixed well depth of $\varepsilon_{sw} = 0.19279$ kcal mol^{-1} and varying solute-water interaction length-scales, σ_{sw}, ranging from 2.0 Å to 15.0 Å. This size range spans the crossover from small to large length-scale hydrophobic hydration as determined by both simulation and theory [2, 24].

As shown earlier, the unbalancing force from LJ attractions dominates that due to long ranged electrostatics at nonpolar interfaces so we focus only on the LJ forces in our analysis of the length scales of hydration. The total renormalized external solute-solvent field is the sum of the bare solute-solvent field and the slowly-varying LMF potential $\phi_{R1}^{LJ}(r)$ in (10), which accounts for unbalanced LJ forces from the nonuniform water (oxygen) density distribution around the solute. It can be written as

$$\phi_R^{LJ}(r) = u_{sw}(r) + \phi_{R1}^{LJ}(r). \tag{12}$$

We compare these potentials for small and large LJ solutes in Fig. 11. At small solute sizes, the renormalized field ϕ_R^{LJ} exhibits a repulsive core nearly identical to that of the bare u_{sw}, and the effective attractions are hardly altered upon renormalization of the potential, indicating only a small unbalanced force around a small solute. The drive to maintain the hydrogen bond network around small solutes dominates the water structure, and solute-water and water-water LJ attractions are found to have little effect on the solvation structure [9].

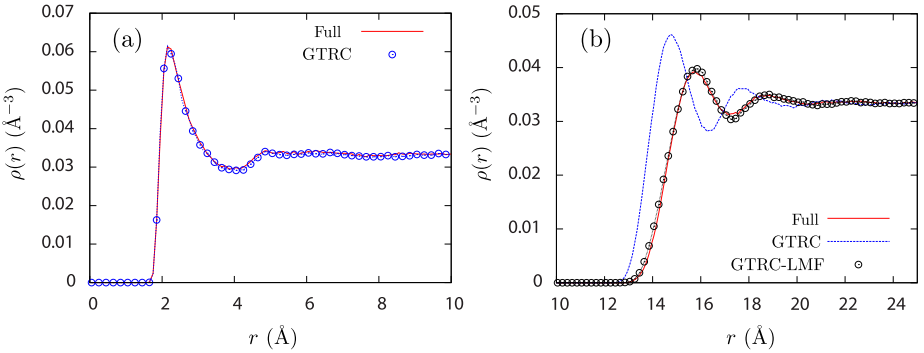

Fig. 12 (Color online) Singlet density distributions of water oxygen sites, $\rho(r)$, around LJ solutes with $\sigma_{sw} = 2.0$ Å (**a**) and $\sigma_{sw} = 15.0$ Å (**b**) for Full and GTRC water models at pressures of $P = 1.0$ atm and $P_0 = P - P_1$, respectively. Data for GTRC water in the presence of the renormalized LMF solute potential is also shown for the large solute (GTRC-LMF)

In contrast, water cannot completely preserve its hydrogen bond network at an interface around a large solute and one hydrogen bond per interfacial water molecule tends to be broken on average [7, 9, 23, 35]. This creates a soft fluctuating interface for which partial drying can be induced by unbalanced attractions from the bulk. These are re-expressed in LMF theory as an effective repulsion pushing water away from the solute surface, as illustrated by the renormalized potential for the large solute in Fig. 11. In order for water to wet such an extended solute surface, this large effective repulsion must be overcome. In hydrophilic surfaces this typically arises from strongly attractive polar groups on the surface, such as hydrogen bonding sites or charged groups, which also can strongly perturb local hydrogen bond configurations.

To illustrate the interplay between unbalanced forces from the bulk, water-water hydrogen-bonding, and the length-scale dependence of hydration, we study the hydration of a small ($\sigma_{sw} = 2.0$ Å) and large ($\sigma_{sw} = 15.0$ Å) LJ solute by SPC/E water and the short-ranged GTRC water model. Since the GTRC model lacks LJ attractions, the unbalancing force from the bulk is absent but the local hydrogen bonding network of water is accurately captured. The GTRC model thus properly describes the dominant crossover behavior of retaining or breaking hydrogen bonds in the small or large length scale regimes, respectively, but the subsequent large length scale interface properties will be incorrect. Comparing GTRC water with the full water model provides more insight into the relative importance of the local network and the unbalancing force on the structuring of water around each solute.

Singlet density distributions of the water oxygen sites around the small and large LJ solute are shown in Figs. 12a and 12b, respectively. In the small solute regime, $\rho(r)$ for GTRC water is essentially identical to that of the full water model. This provides dramatic confirmation of the standard physical picture that small length scale hydrophobicity is almost completely dominated by the need to maintain local hydrogen bonding around the solute. Unbalanced forces from either the LJ or long-ranged Coulomb interaction play essentially no structural role in this regime.

In contrast, although the GTRC model correctly describes the necessary breaking of local hydrogen bonds around a large solute in Fig. 12b the details of the resulting interface profile are very different from that of the full water model. Removal of LJ attractions in GTRC water eliminates the large effective repulsion at the extended solute surface, and uncorrected GTRC water appears to wet the surface of the nonpolar solute. However, the interface is soft

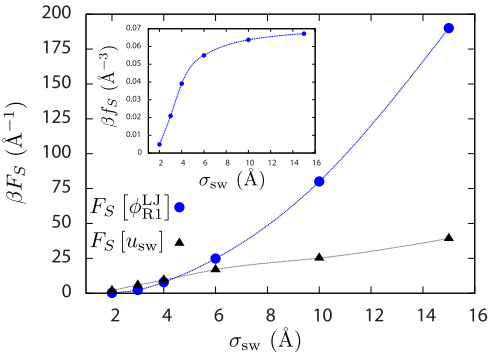

Fig. 13 (Color online) Components of the mean solvation force F_S due to ϕ_{R1}^{LJ} and u_{sw} as a function of the solute-water interaction length scale, σ_{sw}. The inset displays the solvation force due to ϕ_{R1}^{LJ} scaled by the surface area of the solute

and when the unbalanced force from ϕ_{R1}^{LJ} in Fig. 10 as given by LMF theory is also taken into account, depletion and the correct structuring of water at the solute surface is very accurately described by the GTRC-LMF curve in Fig. 12b.

Although the qualitative dependence of the unbalanced force on solvation length scale is depicted in Fig. 11, a more quantitative metric of this behavior is desirable. To that end, we introduce the mean solvation force acting on water due to the renormalized LJ solute external field,

$$F_S\left[\phi_R^{LJ}\right] = -\int d\mathbf{r}\,\rho(r)\frac{\partial u_{sw}(r)}{\partial r} - \int d\mathbf{r}\,\rho(r)\frac{\partial \phi_{R1}^{LJ}(r)}{\partial r}$$
$$= F_S[u_{sw}] + F_S\left[\phi_{R1}^{LJ}\right]. \tag{13}$$

As illustrated in Fig. 13, the unbalanced force due to water-water LJ attractions dominates in the large-scale regime, and can only be overcome by unphysically large solute-water LJ attractions. In the small scale regime, solute-water attractions are comparable in magnitude to the unbalancing force, and can be larger for certain solute sizes (the relative magnitudes are dependent upon the value of ε_{sw}). However, as the GTRC model shows, the important physics in this regime is simply maintaining the hydrogen bond network, and this imposes a near constant solvation structure as the water-solute attractions are varied [9, 17].

Upon normalizing the mean unbalanced force by the surface area of the solute,

$$f_S\left[\phi_{R1}^{LJ}\right] = F_S\left[\phi_{R1}^{LJ}\right]/4\pi\sigma_{sw}^2, \tag{14}$$

a transition from scaling of F_S with solute volume to scaling with surface area occurs at the small to large length scale solvation crossover length of roughly 10 Å, as evidenced by the plateau in f_S depicted in the inset of Fig. 13. This plateau is similar to that which occurs in the solvation free energy [18, 24], and provides another indicator of the transition from small to large length scale hydrophobicity.

5 Conclusions

In this work, we have examined the different roles of short and long ranged forces in the determination of the structure and thermodynamics of uniform and nonuniform aqueous systems, using concepts inherent in classical perturbation and LMF theory. In particular, we have evaluated individually for SPC/E water the contributions of (i) all the strong short

ranged repulsive and attractive interactions that lead to the local hydrogen-bonding network, (ii) longer ranged dispersive LJ attractions between molecules, and (iii) long ranged dipole-dipole interactions, and demonstrated a hierarchical ordering of their importance in determining several properties of water in uniform and nonuniform systems.

All of our truncated models accurately describe the local hydrogen bonding network, and as expected, this network alone is sufficient to match bulk structure as well as solvent structure around small hydrophobic solutes provided that the bulk density and temperature are accurately prescribed. Furthermore, the anomalous temperature and density dependence of the "internal pressure" of water is found to be dominated by the competing short-ranged repulsive and attractive forces determining the local hydrogen bonding network as well.

But local network concepts alone cannot capture all the complexities of even the simple SPC/E water model. While the dispersive LJ attractions between water molecules primarily provide a uniform cohesive energy in bulk systems, they strongly influence the structure and density profile of large scale hydrophobic interfaces. Their importance provides further support for analogies between water at extended hydrophobic interfaces and the liquid-vapor interface, and the unbalanced LJ force can be used to quantify the transition between small and large scale hydrophobicity for simple solutes.

Although the long-ranged dipolar interactions between molecules have only small effects on most of the interfacial density properties considered here, we have shown elsewhere that they are crucial in determining dielectric properties of both bulk and nonuniform water. Indeed, as will be discussed elsewhere, we have found that electrostatic quantities may in fact be a sensitive structural probe of hydrophobicity in general environments [27].

This interaction hierarchy, wherein strong short-ranged local interactions alone determine structure in uniform environments while the longer ranged forces are needed as well to capture other properties could prove quite useful in refining simple site-site water models. Current water models incorporate a vast amount of clever engineering and empirical fine-tuning and manage to reproduce a variety of different properties through a complex balance of competing interactions with simple functional forms. Changes in the potential that improve one property generally speaking produce poorer results for several others.

One promising route to a more systematic procedure may be sensitivity analysis, in which small perturbations of potential parameters are made and the correlated response of a variety of physical observables is quantified. By perturbing the relative magnitudes of short and long ranged interactions, Iordanov et al. found that thermodynamic properties of bulk water are most sensitive to small changes in the LJ repulsions and the short ranged electrostatic interactions [19], in agreement with our findings. A new water model was then proposed by optimizing parameters to reproduce a specific bulk thermodynamic quantity (the internal energy) in an attempt to correct the deficiencies present in a previously developed water potential.

However, the theoretical scheme of splitting the potential described in this paper may provide a more concrete and physically suggestive path to incrementally match various known physical quantities for water without ruining the fitting of previous quantities, and one could combine an approach like sensitivity analysis with the conceptual framework presented herein to systematically optimize a specific water model.

In particular, it has recently been suggested that the accuracy with which a water model can predict the experimental T_{MD} correlates well with the accuracy that the same model displays in predicting the thermodynamics of small-scale hydrophobic hydration [3]. Arguably, the least justified feature of current simple water models like SPC/E is the functional form of the core LJ potential $u_0(r)$, especially at the very short separations relevant for describing local hydrogen bonding as illustrated in Fig. 2. One could try to fine-tune a GTRC-type

model through alteration of the local hydrogen bond network by varying the form of the repulsive core in order to match the experimental density maximum, as well as other bulk properties like the internal pressure, in order to obtain a short-ranged system that yields accurate bulk properties. Although a detailed discussion of this process is beyond the scope of this article, one could try to use some type of optimization procedure to determine such potentials [19, 26, 45]. Perhaps first principles DFT simulations [21, 32] could be used to provide a more fundamental description of the local network. Subsequently, the structure and thermodynamics of nonuniform systems, which require dispersions and long ranged Coulomb interactions, could be used to parametrize the long-ranged interactions.

This work was supported by the National Science Foundation (grants CHE0628178 and CHE0848574). We are grateful to Lawrence Pratt and Shule Liu for helpful remarks. We also thank an anonymous reviewer for bringing Refs. [21] and [32] to our attention.

6 Simulation Details

All molecular dynamics simulations were performed using modified versions of the DL_POLY software package [34] and the SPC/E water model [6] or its variants described in Sect. 2. The equations of motion were integrated using the leapfrog algorithm with a timestep of 1 fs [1] while maintaining constant temperature and pressure conditions through the use of a Berendsen thermostat and barostat respectively [5].

6.1 Bulk Water Simulations

The evaluation of electrostatic interactions in bulk simulations of the full SPC/E water model employed the standard Ewald summation method using a real space cutoff of 9.5 Å, unless this was larger than half of the box length, in which case the cutoff was set to half of the box length [1]. Short-ranged electrostatic interactions in the GT and GTRC reference systems, as well as LJ interactions in all systems, were truncated at the real space cutoff length used in the analogous full system. Simulations of bulk water were performed with $N = 1000$ molecules in the isothermal-isobaric (NPT) ensemble to determine the density maximum and with $N = 256$ molecules in the canonical (NVT) ensemble to determine $P(T)$ and the internal pressure. The duration of equilibration and production runs, as well as the temperatures sampled are listed in Table 1. The internal pressure in (7) was calculated by evaluating $\varepsilon(v)$ for numerous values of v at each T. The function $\varepsilon(v)$ was then fit to a polynomial, which was differentiated at the desired v to yield the internal pressure.

6.2 Simulation of Nonuniform Systems

In order to generate starting configurations for the LV and LS interfacial systems discussed in Sect. 5, we first equilibrated N water molecules in a cubic geometry, where N is listed in Table 1. The z-dimension of the system was then elongated to more than three times the x- and y-dimensions, and in the case of the LS interface, a wall potential of the form

$$U_w(z) = \frac{A}{|z - z_w|^9} - \frac{B}{|z - z_w|^3} \tag{15}$$

was added at $z_w = 0$ and the parameters A and B are given in Ref. [22]. In order to ensure water molecules did not approach the wall from $z < 0$, a repulsive wall was added at large z to constrain the water molecules to the desired region of the simulation cell while still

Table 1 Details of the MD simulations performed in this work. N and T refer to the number of water molecules and the temperature of the system, respectively. The equilibration times and data collection times are denoted by t_{equil} and t_{run}, respectively

System	N	T	t_{equil}	t_{run}
Bulk Water	256	220–340 K	5 ns	5 ns
Bulk Water	1000	220–300 K	2 ns	2 ns
LV Interface	1728	298 K	1 ns	500 ps
LS Interface	2468	298 K	1 ns	500 ps
Small LJ Solutes ($\sigma_{\text{sw}} < 10$ Å)	1000	298 K	2 ns	2 ns
Large LJ Solutes ($\sigma_{\text{sw}} \geq 10$ Å)	6000	298 K	1 ns	1 ns

allowing a large vacuum region for the formation of a vapor phase. Electrostatic interactions were handled using the corrected Ewald summation method for slab geometries [44] with a real space cutoff of 11.0 Å, which was also the cutoff distance for LJ and short-ranged electrostatic interactions.

Molecular dynamics simulations of the hydration of LJ solutes were performed in the NPT ensemble using standard Ewald summation to evaluate the electrostatic interactions, with a real space cutoff of 11.0 Å. The short ranged v_0 potential and the water-water LJ potential were also truncated at 11.0 Å. The LJ solute was represented by a fixed external potential centered at the origin, and the solute-water interactions were truncated at one-half the length of the simulation cell. The number of molecules and simulation times are listed in Table 1.

References

1. Allen, M.P., Tildesley, D.J.: Computer Simulation of Liquids. Oxford, New York (1987)
2. Ashbaugh, H.S.: Entropy crossover from molecular to macroscopic cavity hydration. Chem. Phys. Lett. **477**, 109–111 (2009)
3. Ashbaugh, H.S., Collett, N.J., Hatch, H.W., Staton, J.A.: Assessing the thermodynamic signatures of hydrophobic hydration for several common water models. J. Chem. Phys. **132**, 124504 (2010)
4. Ben-Naim, A., Stillinger, F.H.: Water and Aqueous Solutions: Structure, Thermodynamics, and Transport Processes. Wiley-Interscience, New York (1972)
5. Berendsen, H.J.C., Postma, J.P.M., van Gunsteren, W.F., DiNiola, A., Haak, J.R.: Molecular dynamics with coupling to an external bath. J. Chem. Phys. **81**, 3684 (1984)
6. Berendsen, H.J.C., Grigera, J.R., Straatsma, T.P.: The missing term in effective pair potentials. J. Phys. Chem. **91**, 6269–6271 (1987)
7. Berne, B.J., Weeks, J.D., Zhou, R.: Dewetting and hydrophobic interaction in physical and biological systems. Annu. Rev. Phys. Chem. **60**, 85–103 (2009)
8. Buldyrev, S.V., Kumar, P., Debenedetti, P.G., Rossky, P.J., Stanley, H.E.: Water-like solvation thermodynamics in a spherically symmetric solvent model with two characteristic lengths. Proc. Natl. Acad. Sci. USA **104**, 20177–20182 (2007)
9. Chandler, D.: Interfaces and the driving force of hydrophobic assembly. Nature **437**, 640–647 (2005)
10. Chen, Y.G., Weeks, J.D.: Local molecular field theory for effective attractions between like charged objects in systems with strong Coulomb interactions. Proc. Natl. Acad. Sci. USA **103**, 7560 (2006)
11. Chen, Y.G., Kaur, C., Weeks, J.D.: Connecting systems with short and long ranged interactions: local molecular field theory for ionic fluids. J. Phys. Chem. B **108**, 19874 (2004)
12. Denesyuk, N.A., Weeks, J.D.: A new approach for efficient simulation of Coulomb interactions in ionic fluids. J. Chem. Phys. **128**, 124109 (2008)
13. Goharshadi, E.K., Morsali, A., Mansoori, G.A.: A molecular dynamics study on the role of attractive and repulsive forces in internal energy, internal pressure and structure of dense fluids. Chem. Phys. **331**, 332–338 (2007)

14. Guillot, B.: A reappraisal of what we have learnt during three decades of computer simulations of water. J. Mol. Liq. **101**, 219–260 (2002)
15. Hansen, J.P., McDonald, I.R.: Theory of Simple Liquids, 3rd edn. Academic Press, New York (2006)
16. Haynes, W.M. (ed.): CRC Handbook of Chemistry and Physics, 91st edn. (Internet Version 2011). CRC Press/Taylor and Francis, Boca Raton (2011)
17. Huang, D.M., Chandler, D.: The hydrophobic effect and the influence of solute-solvent attractions. J. Phys. Chem. B **106**, 2047–2053 (2002)
18. Huang, D.M., Geissler, P.L., Chandler, D.: Scaling of hydrophobic solvation free energies. J. Phys. Chem. B **105**, 6704–6709 (2001)
19. Iordanov, T.D., Schenter, G.K., Garrett, B.C.: Sensitivity analysis of thermodynamic properties of liquid water: a general approach to improve empirical potentials. J. Phys. Chem. A **110**, 762–771 (2006)
20. Jirsák, J., Nezbeda, I.: Molecular mechanisms underlying the thermodynamics properties of water. J. Mol. Liq. **134**, 99–106 (2007)
21. Kuo, I.-F.W., Mundy, C.J., Eggimann, B.L., McGrath, M.J., Siepmann, J.I., Chen, B., Vieceli, J., Tobias, D.J.: Structure and dynamics of the aqueous liquid-vapor interface: a comprehensive particle-based simulation study. J. Phys. Chem. B **110**, 3738–3746 (2006)
22. Lee, S.H., Rossky, P.J.: A comparison of the structure and dynamics of liquid water at hydrophobic and hydrophilic surfaces—a molecular dynamics simulation study. J. Chem. Phys. **100**, 3334–3345 (1994)
23. Lee, C.Y., McCammon, J.A., Rossky, P.J.: The structure of liquid water at an extended hydrophobic surface. J. Chem. Phys. **80**, 4448–4455 (1984)
24. Lum, K., Chandler, D., Weeks, J.D.: Hydrophobicity at small and large length scales. J. Phys. Chem. B **103**, 4570–4577 (1999)
25. Luzar, A., Chandler, D.: Effect of environment on hydrogen bond dynamics in liquid water. Phys. Rev. Lett. **76**, 928–931 (1996)
26. Marcotte, E., Stillinger, F.H., Torquato, S.: Optimized monotonic convex pair potentials stabilize low-coordinated crystals. Soft Matter **7**, 2332–2335 (2011)
27. Remsing, R.C., Rodgers, J.M., Weeks, J.D.: Unpublished
28. Rodgers, J.M., Weeks, J.D.: Interplay of local hydrogen-bonding and long-ranged dipolar forces in simulations of confined water. Proc. Natl. Acad. Sci. USA **105**, 19136 (2008)
29. Rodgers, J.M., Weeks, J.D.: Local molecular field theory for the treatment of electrostatics. J. Phys., Condens. Matter **20**, 494206 (2008)
30. Rodgers, J.M., Weeks, J.D.: Accurate thermodynamics for short-ranged truncations of Coulomb interactions in site-site molecular models. J. Chem. Phys. **131**, 244108 (2009)
31. Rodgers, J.M., Hu, Z., Weeks, J.D.: On the efficient and accurate short-ranged simulations of uniform polar molecular liquids. Mol. Phys. **109**, 1195–1211 (2011)
32. Schmidt, J., VandeVondele, J., Kuo, I.-F.W., Sebastiani, D., Siepmann, J.I., Hutter, J., Mundy, C.J.: Isobaric-isothermal molecular dynamics simulations utilizing density functional theory: an assessment of the structure and density of water at near-ambient conditions. J. Phys. Chem. B **113**, 11959–11964 (2009)
33. Shah, J.K., Asthagiri, D., Pratt, L.R., Paulaitis, M.E.: Balancing local order and long-ranged interactions in the molecular theory of liquid water. J. Chem. Phys. **127**, 144508 (2007)
34. Smith, W., Yong, C., Rodger, P.: DL_POLY: application to molecular simulation. Mol. Simul. **28**, 385–471 (2002)
35. Stillinger, F.H.: Structure in aqueous solutions of nonpolar solutes from the standpoint of scaled-particle theory. J. Solution Chem. **2**, 141–158 (1973)
36. Varilly, P., Patel, A.J., Chandler, D.: An improved coarse-grained model of solvation and the hydrophobic effect. J. Chem. Phys. **134**, 074109 (2011)
37. Vega, C., Abascal, J.L.F., Conde, M.M., Aragones, J.L.: What ice can teach us about water interactions: a critical comparison of the performance of different water models. Faraday Discuss. **141**, 251–276 (2009)
38. Wang, J., Román-Pérez, G., Soler, J.M., Artacho, E., Fernández-Serra, M.-V.: Density, structure, and dynamics of water: the effect of van der Waals interactions. J. Chem. Phys. **134**, 024516 (2011)
39. Weeks, J.D.: Connecting local structure to interface formation: a molecular scale van der Waals theory of nonuniform liquids. Annu. Rev. Phys. Chem. **53**, 533–562 (2002)
40. Weeks, J.D., Chandler, D., Andersen, H.C.: Role of repulsive forces in determining the equilibrium structure of simple liquids. J. Chem. Phys. **54**, 5237–5247 (1971)
41. Widom, B.: Intermolecular forces and the nature of the liquid state. Science **157**, 375–382 (1967)
42. Xu, L., Buldyrev, S.V., Angell, C.A., Stanley, H.E.: Thermodynamics and dynamics of the two-scale spherically symmetric Jagla ramp model of anomalous liquids. Phys. Rev. E **74**, 031108 (2006)
43. Yan, Z., Buldyrev, S.V., Giovambattista, N., Stanley, H.E.: Structural order for one-scale and two-scale potentials. Phys. Rev. Lett. **95**, 130604 (2005)

44. Yeh, I.C., Berkowitz, M.L.: Ewald summation for systems with slab geometry. J. Chem. Phys. **111**, 3155–3162 (1999)
45. Zhu, S.B., Wong, C.F.: Sensitivity analysis of water thermodynamics. J. Chem. Phys. **98**, 8892–8899 (1993)